An On-Demand Coherent Single-Electron Source
G. Fève, *et al.*
Science **316**, 1169 (2007);
DOI: 10.1126/science.1141243

6. F. Bournaud, P.-A. Duc, P. Amram, F. Combes, J.-L. Gach, *Astron. Astrophys.* **425**, 813 (2004).
7. P.-A. Duc, F. Bournaud, F. Masset, *Astron. Astrophys.* **427**, 803 (2004).
8. C. Mendes de Oliveira, H. Plana, P. Amram, C. Balkowski, M. Bolte, *Astron. J.* **121**, 2524 (2001).
9. J. F. Navarro, C. S. Frenk, S. D. M. White, *Astropys. J.* **462**, 563 (1996).
10. F. Nicastro *et al.*, *Nature* **433**, 495 (2005).
11. R. Cen, J. P. Ostriker, *Astrophys. J.* **650**, 560 (2006).
12. F. Bournaud, P.-A. Duc, *Astron. Astrophys.* **456**, 481 (2006).
13. D. N. Spergel *et al.*, *Astrophys. J.* **148** (Supp.), 175 (2003).
14. M. Rauch, *Annu. Rev. Astron. Astrophys.* **36**, 267 (1998).
15. D. Pfenniger, F. Combes, L. Martinet, *Astron. Astrophys.* **285**, 79 (1994).
16. I. A. Grenier, J.-M. Casandjian, R. Terrier, *Science* **307**, 1292 (2005).
17. B. K. Malphrus, C. E. Simpson, S. T. Gottesman, T. G. Hawarden, *Astron. J.* **114**, 1427 (1997).
18. P.-A. Duc, I. F. Mirabel, *Astron. Astrophys.* **333**, 813 (1998).
19. The National Radio Astronomy Observatory is a facility of the NSF operated under cooperative agreement by Associated Universities, Inc.
20. J. Braine *et al.*, *Astron. Astrophys.* **378**, 51 (2001).
21. S. J. Higdon, J. L. Higdon, J. Marshall, *Astrophys. J.* **640**, 768 (2006).
22. F. Bournaud, F. Combes, *Astron. Astrophys.* **401**, 817 (2003).
23. Materials and methods are available as supporting material on *Science* Online.
24. H. Flores, F. Hammer, M. Puech, P. Amram, C. Balkowski, *Astron. Astrophys.* **455**, 107 (2006).
25. The confidence level is evaluated assimilating the uncertainties on all parameters and on the method itself (assuming Gaussian statistics) and combining them as independent variables.
26. M. L. Mateo, *Annu. Rev. Astron. Astrophys.* **36**, 435 (1998).
27. V. Springel, C. S. Frenk, S. D. M. White, *Nature* **440**, 1137 (2006).
28. M. Boquien *et al.*, *Astron. Astrophys.* **467**, 93 (2007).
29. L. J. Sage, S. N. Shore, P. M. Solomon, *Astrophys. J.* **351**, 422 (1990).
30. P. Maloney, J. H. Black, *Astrophys. J.* **325**, 389 (1988).
31. J. Braine, F. Herpin, *Nature* **432**, 369 (2004).
32. F. P. Israël *et al.*, *Astron. Astrophys.* **406**, 817 (2003).
33. J. L. Donley *et al.*, *Mon. Not. R. Astron. Soc.* **369**, 1741 (2006).

34. The numerical simulations were carried out at CEA/Centre de Calcul Recherche et Technologie and CNRS/Institute du Développement et des Ressources en Informatique Scientifique. Numerical models have benefited from input from the collaboration HORIZON, and we thank F. Combes and R. Teyssier. We thank J. Braine, P. Weilbacher, I. Grenier, Y. Revaz, F. Boulanger, and F. Hammer for valuable comments on the dynamical analysis and/or general results. We made use of data from the Digitized Sky Survey, produced at the Space Telescope Science Institute under U.S. Government grant NAG W-2166.

Supporting Online Material

www.sciencemag.org/cgi/content/full/1142114/DC1
Materials and Methods
Figs. S1 to S8
Table S1
References

5 March 2007; accepted 20 April 2007
Published online 10 May 2007;
10.1126/science.1142114
Include this information when citing this paper.

An On-Demand Coherent Single-Electron Source

G. Fève,[1] A. Mahé,[1] J.-M. Berroir,[1] T. Kontos,[1] B. Plaçais,[1] D. C. Glattli,[1,2]* A. Cavanna,[3] B. Etienne,[3] Y. Jin[3]

We report on the electron analog of the single-photon gun. On-demand single-electron injection in a quantum conductor was obtained using a quantum dot connected to the conductor via a tunnel barrier. Electron emission was triggered by the application of a potential step that compensated for the dot-charging energy. Depending on the barrier transparency, the quantum emission time ranged from 0.1 to 10 nanoseconds. The single-electron source should prove useful for the use of quantum bits in ballistic conductors. Additionally, periodic sequences of single-electron emission and absorption generate a quantized alternating current.

In quantum optics, a single-photon source is an essential building block for the manipulation of the smallest amount of information coded by a quantum state: a qubit (*1*, *2*). Combined with beam splitters, polarizers, and projective measurements, several photonic qubits can be manipulated to process quantum information (*3*). The most celebrated case is the secure transmission of information by means of quantum cryptography. Similarly, one expects that electrons propagating ballistically in ultrapure low-dimensional conductors can perform quantum logic tasks in perfect analogy with photons propagating in optical media (*4*–*6*). The analogy has a long history (*7*) and has provided illuminating comparisons between the intensity of light and that of electrical current; between photon noise and electrical shot noise (*8*, *9*); and, more recently, between photon and electron quantum entanglement (*10*–*12*). Because electrons are fermions, entanglement offers new routes not possible with photons (*12*). Practically, electronic analogs of beam splitters and Fabry-Pérot and Mach-Zehnder interferometers (*13*, *14*) have been used in ballistic conductors, providing the necessary quantum gate for an all-linear electron optics quantum computation. Yet missing were a single-electron source and a single-electron detector (*15*) suitable for coherent emission and projective measurements. The former initializes quantum states, whereas the latter reads the final states after electrons have passed through the quantum gates.

Unlike the case of photons, the creation of single-electron sources is expected to be simpler because of Fermi statistics and Coulomb interaction. For example, considering a voltage-biased single-mode conductor, a contact at energy eV above the energy of the other contact is known to inject single electrons into the conductor at a regular rate eV/h, thereby leading to the quantization of dc conductance in quantum point contacts (QPCs) (*16*, *17*). A second example is the electron pump, in which a dc current is produced by sequential time-controlled transfer of single electrons between metallic islands in series (*18*, *19*) or by the manipulation of tunnel barriers of quantum dots (*20*, *21*). The cost in Coulomb charging energy to add or remove an electron ensures a well-defined electron number in each island or dot. These two sources are, however, not useful for quantum information. In the first case, there is no time control of the electron injection. Because only statistical measurements are possible, the biased contact is suitable for demonstrating coherent phenomena such as interferences or electron entanglement (*10*, *11*) but not for manipulating quantum information. In the second example, time-controlled injection can be realized, but the energy of emitted electrons is expected to spread, at random, in an energy range much larger than the tunneling rate (typically a fraction of the charging energy, depending on the pumping conditions). The statistical distribution in energy will smear the coherent effects required for manipulating the quantum information. Finally, a third approach has been theoretically proposed in (*22*–*24*), considering voltage pulses $V(t)$ applied to an ohmic contact. When the Faraday flux $e\int V(t')dt'/h$ is an integer, an integer number of electrons is injected. Here noiseless injection requires that the pulses have a special Lorenzian shape and exact integer Faraday flux, otherwise logarithmic divergence of the charge fluctuations occurs. No experiment is available yet to test these ideas.

We report here on the realization of a time-controlled single-electron source suitable for the coherent manipulation of ballistic electronic qubits, which emits the electrons into a well-defined quantum state. The injection scheme is different from those considered above. The source is made of a quantum dot, realized in a two-dimensional (2D) electron gas in gallium arsenide (GaAs) semiconductors and tunnel-coupled to the conductor through a QPC. By application of a sudden voltage step on a capacitively coupled gate, the charging energy is

[1]Laboratoire Pierre Aigrain, Département de Physique de l'Ecole Normale Supérieure, 24 rue Lhomond, 75231 Paris Cedex 05, France. [2]Service de Physique de l'Etat Condensé, CEA Saclay, F-91191 Gif-sur-Yvette, France. [3]Laboratoire de Photonique et Nanostructures, UPR20 CNRS, Route de Nozay, 91460 Marcoussis Cedex, France.

*To whom correspondence should be addressed. E-mail: glattli@lpa.ens.fr

compensated for and the electron occupying the highest energy level of the dot is emitted. The final state of the electron is a coherent wave packet propagating away in the conductor. Its energy width is given by the inverse tunneling time, as required for an on-demand single-particle source, and is independent of temperature. Its mean energy can be adjusted above the Fermi energy by tuning the voltage step amplitude. The circuit (Fig. 1A), is realized in a 2D electron gas in a GaAsAl/GaAs heterojunction of nominal density $n_s = 1.7 \times 10^{15}$ m^{-2} and mobility $\mu = 260$ V^{-1} m^2 s^{-1}. The dot is electrostatically coupled to a metallic top gate, 100 nm above the 2D electron gas, whose ac voltage, V_{exc}, controls the dot potential at the subnanosecond time scale. For all measurements, the electronic temperature is about 200 mK and a magnetic field $B \approx 1.3$ T is applied to the sample so as to work in the quantum Hall regime with no spin degeneracy. The QPC dc gate voltage V_G is tuned to control the transmission D of a single edge state as well as the dc dot potential. As reported (*25*), this circuit constitutes the paradigm of a quantum-coherent resistor-capacitor (RC) circuit, where coherence is seen to strongly affect the charge relaxation dynamics. From this study, the charging energy $\Delta + e^2/C \approx \Delta \approx 2.5$ K was extracted (*26*). Here the large top-gate capacitance makes the Coulomb energy e^2/C unusually small, and the total charging energy reduces to the energy-level spacing Δ.

In (*25*), the linear response of the current to the ac top-gate voltage was investigated, and the ac charge amplitude was much lower than the elementary charge e. In order to achieve single-charge injection, we had to apply a high-amplitude excitation ($V_{exc} \sim \Delta/e$) and go beyond the linear regime. When an electron is suddenly brought above the Fermi energy of the lead, it is expected to escape the dot at a typical tunnel rate $\tau^{-1} = D\Delta/h$, where Δ/h is the attempt frequency and D is the transmission probability. This gives nanosecond time scales, for which single-charge detection is still out of reach experimentally. To increase the signal-to-noise ratio, a statistical average over many individual events is used by generating repetitive sequences of single-electron emission followed by single-electron absorption (or hole emission) as shown in Fig. 1A. This is done by applying a periodic square wave voltage amplitude $\approx \Delta/e$ to the top gate. Figure 1B shows typical temporal traces of the current averaged over a few seconds for a repetition period of $T = 32$ ns. The single-electron events reconstruct the exponential current decay of an RC circuit. When transmission D is decreased from ≈0.03 to ≈0.002, the relaxation time τ, extracted from the exponential decay, increases from 0.9 to 10 ns. For the two highest transmissions in Fig. 1B, $\tau \ll T/2$, the current decays to zero, and the mean transferred charge per half period is constant. For the smallest transmission, $\tau \sim T/2$, the mean emitted charge decreases because electrons have reduced probability of escaping the dot. These time-domain measurements are limited by the 1-GHz bandwidth of the acquisition card and give access to the few-nanosecond injection times corresponding to small transmissions $D \lesssim 0.03$.

In order to get a better understanding of the above results, we extend the harmonic linear re-

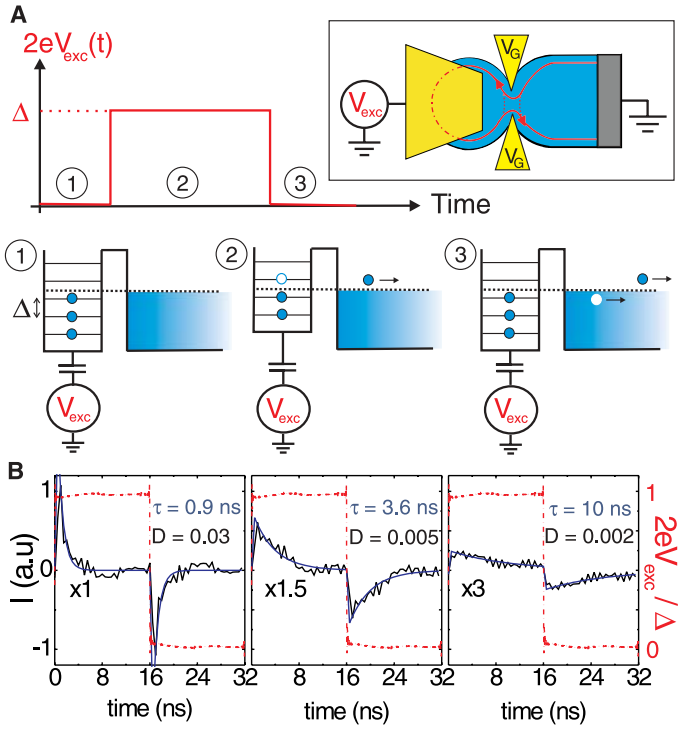

Fig. 1. Single-charge injection. (**A**) Schematic of single-charge injection. Starting from an antiresonant situation where the Fermi energy lies between two energy levels of the dot (step 1), the dot potential is increased by Δ moving one occupied level above the Fermi energy (step 2). One electron then escapes the dot on the mean time $\tau = h/D\Delta$. The dot potential is then brought back to its initial value (step 3), where one electron can enter it, leaving a hole in the Fermi sea. (Inset at right) The quantum RC circuit: one edge channel is transmitted inside the submicrometer dot, with transmission D tuned by the QPC gate voltage V_G. The dot potential is varied by a radio-frequency excitation V_{exc} applied on a macroscopic gate located on top of the dot. The electrostatic potential can also be tuned by V_G because of the electrostatic coupling between the dot and the QPC. (**B**) Time-domain measurement of the average current (black curves) on one period of the excitation signal (red curves) at $2eV_{exc} = \Delta$ for three values of the transmission D. The relaxation time τ is deduced from an exponential fit (blue curve).

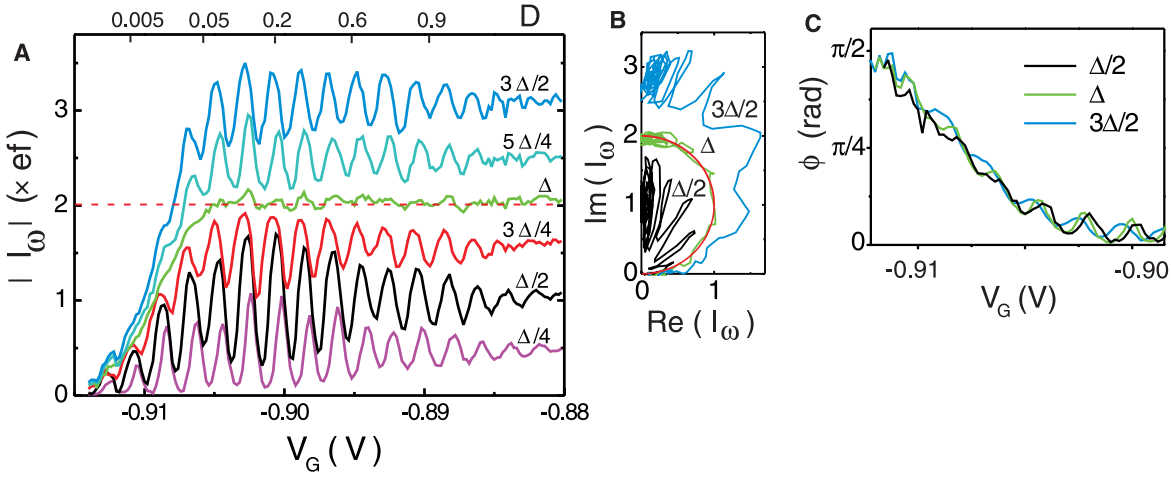

Fig. 2. I_ω as a function of V_G at $f = 180$ MHz for different values of the excitation amplitude $2eV_{exc}$. Transmission D is also indicated. (**A**) Modulus $|I_\omega|$. The horizontal dashed line is the constant value $|I_\omega| = 2ef$. (**B**) Nyquist representation (imaginary part of I_ω versus real part of I_ω). The red curve corresponds to an RC circuit of constant capacitance e^2/Δ and varying resistance. (**C**) Phase ϕ. The phase ϕ is independent of V_{exc}.

sponse theory of a quantum RC circuit (*27*–*29*) to calculate the nonlinear response to a high-amplitude square excitation voltage ($eV_{exc} >> hf$). Calculation shows that the circuit still behaves as an RC circuit with a current given by

$$I(t) = \frac{q}{\tau} e^{-t/\tau} \text{ for } 0 \le \tau \le T/2 \quad (1)$$

$$q = e \int d\varepsilon N(\varepsilon)[f(\varepsilon - 2eV_{exc}) - f(\varepsilon)] \quad (2)$$

$$\tau = \frac{h}{2} \frac{\int d\varepsilon N(\varepsilon)^2 [f(\varepsilon - 2eV_{exc}) - f(\varepsilon)]}{\int d\varepsilon N(\varepsilon)[f(\varepsilon - 2eV_{exc}) - f(\varepsilon)]} \quad (3)$$

where $N(\varepsilon)$ is the dot density of states and $f(\varepsilon)$ denotes the Fermi-Dirac distribution. The nonlinear capacitance and charge relaxation resistance can be defined respectively by $\tilde{C}_q \equiv q/2V_{exc}$ and $\tilde{R}_q \equiv \tau/\tilde{C}_q$. For unit transmission $D = 1$, electrons are fully delocalized, $N(\varepsilon)$ is uniform, and the charge q evolves linearly with V_{exc} as expected. In contrast, for low transmission, $N(\varepsilon)$ is sharply peaked on well-resolved energy levels, and q exhibits a staircase dependence on V_{exc}, with steep steps whenever one electronic level is brought above the Fermi energy. Thus, our calculations establish the process of single-electron injection depicted in Fig. 1. For a dot energy spectrum with constant level spacing Δ, a remarkable situation occurs when $2eV_{exc} = \Delta$, as $q = e$ and $\tilde{C}_q = e^2/\Delta$ irrespective of the transmission D and of the dc dot potential. As a matter of fact, Eq. 2 shows that, in these conditions, q is given by integrating $N(\varepsilon)$ over exactly one level spacing. For $D << 1$, we recover the Landauer formula for the resistance $\tilde{R}_q = h/De^2$, and the escape time is given by $\tau = h/D\Delta$, as expected from a semiclassical approach. The exponential current decay, the constant injection charge for $\tau << T/2$, and the decrease of τ with transmission D account well for our experimental observations in Fig. 1B.

For a more accurate experimental determination of q and τ and to investigate subnanosecond time scales, we consider in the following measurements the current first harmonic I_ω at higher frequencies $f = \omega/2\pi = 1/T$. Following Eq. 1, we have

$$I_\omega = \frac{2qf}{1 - i\omega\tau} \quad (4)$$

so that the modulus $|I_\omega|$ and the phase ϕ [$\tan(\phi) = \omega\tau$] allow for the determination of q and τ.

Figure 2A shows $|I_\omega|$ measured as a function of QPC gate voltage V_G at $f = 180$ MHz for increasing values of the excitation voltage $2eV_{exc}$. The range of V_G maps the full transmission excursion $D = 0$ to 1. The low-excitation $2eV_{exc} = \Delta/4$ data nearly correspond to the linear response reported in (*25*). The current exhibits strong oscillations reflecting the variation with V_G of the dot density of states at the Fermi energy. At larger excitation voltages, the current peaks are broadened as expected from Eq. 2 when $2eV_{exc}$ gets larger than thermal energy (k_BT). For $2eV_{exc} = \Delta$, the oscillations disappear completely and $|I_\omega| = 2ef$, down to a low transmission threshold $D \sim 0.05$. The oscillations reappear for larger excitations. The constant current $|I_\omega| = 2ef$ is the frequency-domain counterpart of the constant charge regime observed in the time domain, for the injection and absorption of a single electron per half period. The cutoff observed for $D \lesssim 0.02$ corresponds to the limit $\omega\tau \gtrsim 1$, where the escape time τ exceeds $T/2$. The constant $\tilde{C}_q$ regime obtained for $2eV_{exc} = \Delta$ can be viewed in the Nyquist representation of Fig. 2B. The corresponding diagram is the half-circle that is characteristic of an RC circuit with a constant capacitance e^2/Δ and transmission-dependent resistance. In contrast, the curves obtained for larger or smaller excitations exhibit strong capacitance oscillations.

Figure 2C represents the phase $\phi = \arctan(\omega\tau)$ of the current as a function of V_G for different excitation voltages. ϕ shows a quasi-monotonic $\pi/2$ sweep in increasing transmission. The absence of residual oscillations proves that τ is nearly insensitive to the dot potential. As seen in Fig. 2C, τ is also independent of V_{exc}. In Fig. 3, we have gathered the values of $\tau(V_G)$ obtained from 1-GHz–bandwidth time-domain measurements at a 31.25-MHz repetition rate and from frequency-domain measurements at 180 and 515 MHz. The measurements probe a very broad transmission range ($D = 0.002$ to 0.2) corresponding to escape times varying from 10 ns to 100 ps. In the overlapping range, the different independent determinations coincide within error bars, agreeing quantitatively with the prediction $\tau = h/D\Delta$ also represented in Fig. 3, where the dependence $D(V_G)$ is deduced from the linear regime (*25*).

We now discuss the conditions for single-electron injection leading to a good quantization of the ac current as a figure of merit of single-charge injection. Figure 4A represents $|I_\omega|$ as function of V_{exc} for typical values of the dc dot potential at fixed transmissions $D \approx 0.2$ and

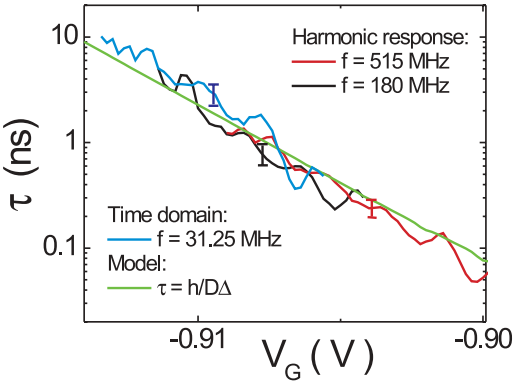

Fig. 3. Escape time τ on a logarithmic scale as a function of QPC gate voltage V_G: experiments (red, blue, and black curves) and model (green curve).

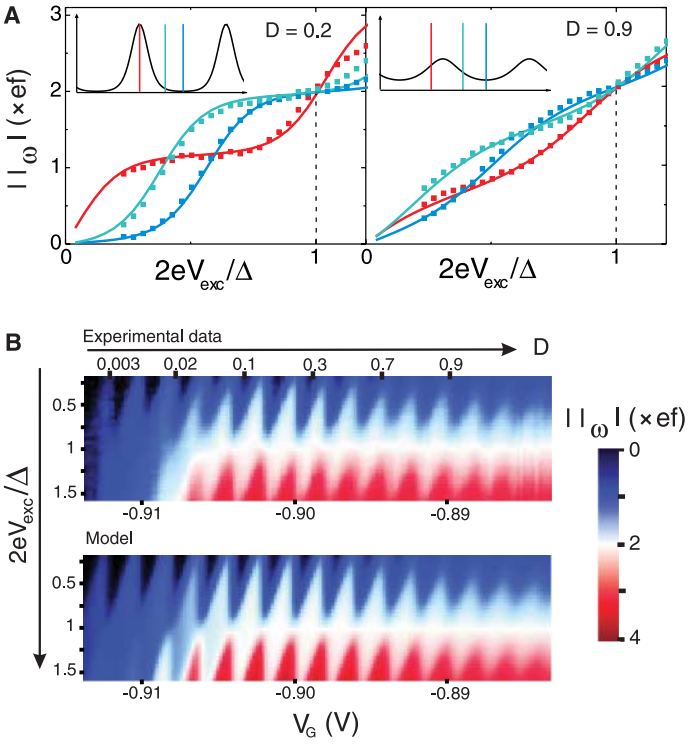

Fig. 4. Quantization of the ac current. (**A**) $|I_\omega|$ as a function of $2eV_{exc}/\Delta$ for different dot potentials at $D \approx 0.2$ (left) and $D \approx 0.9$ (right). Points correspond to experimental values and lines to theoretical predictions. (Insets) Schematic representation of the dot density of states $N(\varepsilon)$. The color bars indicate the dot potential for the corresponding experimental data. (**B**) Color plot of $|I_\omega|$ as a function of $2eV_{exc}/\Delta$ and V_G: experiments (top) and model (bottom).

$D \approx 0.9$. Transmission $D \approx 0.2$ is low enough for the electronic states to be well resolved, as shown in the inset of Fig. 4A (left), but is still large enough for the escape time to be shorter than $T/2$. When the Fermi energy lies exactly in the middle of a density-of-states valley, we observe a well-pronounced $|I_\omega| = 2ef$ current plateau centered on $2eV_{exc} = \Delta$. Whereas the current plateau resolution is noise-limited to better than 1% (for a 10-s acquisition time), the plateau value is determined with an uncertainty of 5% due to systematic calibration error. At this working point, the plateau is robust when the parameters are varied. In contrast, if the Fermi energy lies on a peak, there is still a current plateau, but its value is arbitrary and very sensitive to parameter variations. These two working points illustrate the importance of having a well-defined charge in the dot before injection. In the first case, the charge is well defined and suitable for charge injection. In the second case, the equilibrium dot charge fluctuates. In particular, when the energy level is exactly resonant with the Fermi energy, its mean occupation at equilibrium is 1/2 and the measured value of the plateau is $1/2 \times 2ef = ef$ (Fig. 4A, left). Thus, this working point is not suitable for a single-electron source. When transmission is increased, even for a suitable working point, the dot charge quantization can be lost because of quantum fluctuations. First, the width of the ac current plateaus decreases and finally nearly vanishes for $D \approx 0.9$. For different transmissions, all curves cross at $|I_\omega| = 2ef$ for $2eV_{exc} = \Delta$, reflecting the constant value of $\tilde{C}_q$ discussed above. Finally, domains of good charge quantization are best shown on the 2D color plot of Fig. 4B (top) where the modulus of the current is represented in a color scale. The vertical axis stands for the excitation voltage V_{exc} and the horizontal axis for the gate voltage V_G. The white diamonds correspond to large domains of constant current $|I_\omega| = 2ef$ suitable for single-electron injection. At high transmissions, the diamonds are blurred by dot charge fluctuations as discussed previously. At small transmissions, even when the dot charge quantization is good, current quantization is lost because of the long escape time $\omega\tau >> 1$, and the current goes to zero. At 180 MHz, optimal working conditions are obtained for $D \approx 0.2$. The experimental results in Fig. 4 are compared with our theoretical model (Eqs. 2 and 3) without any adjustable parameter (solid lines in Fig. 4A and lower plot in Fig. 4B) [we use the 1D modeling of our circuit (density of states, transmission, and dot-gates coupling) described in (*25*)]. The agreement between measurements and theoretical predictions is excellent, which shows that our single-electron source lends itself to quantitative modeling.

The availability of a coherent source of single electrons emitted on demand from a single energy level on nanosecond time scales opens the way for a new generation of experiments never possible before. Synchronization of similar sources could be used in the future to probe electron antibunching or electron entanglement in multilead conductors or to generate electronic flying qubits in ballistic conductors.

References and Notes

1. A. Imamoglu, Y. Yamamoto, *Phys. Rev. Lett.* **72**, 210 (1994).
2. N. Gisin, G. Ribordy, W. Tittel, H. Zbinden, *Rev. Mod. Phys.* **74**, 145 (2002).
3. P. Kok *et al.*, *Rev. Mod. Phys.* **79**, 135 (2007).
4. A. Bertoni, P. Bordone, R. Brunetti, C. Jacoboni, S. Reggiani, *Phys. Rev. Lett.* **84**, 5912 (2000).
5. R. Ionicioiu, G. Amaratunga, F. Udrea, *Int. J. Mod. Phys.* **15**, 125 (2001).
6. T. M. Stace, C. H. W. Barnes, G. J. Milburn, *Phys. Rev. Lett.* **93**, 126804 (2004).
7. W. van Haeringen, D. Lenstra, *Analogies in Optics and Micro Electronics* (Kluwer, Dordrecht, Netherlands, 1990).
8. M. Büttiker, *Phys. Rev. B* **46**, 12485 (1992).
9. Ya. M. Blanter, M. Büttiker, *Phys. Rep.* **336**, 2 (2000).
10. C. W. J. Beenakker, C. Emary, M. Kindermann, J. L. van Velsen, *Phys. Rev. Lett.* **91**, 147901 (2003).
11. P. Samuelsson, E. V. Sukhorukov, M. Büttiker, *Phys. Rev. Lett.* **92**, 026805 (2004).
12. C. W. J. Beenakker, in *Quantum Computers, Algorithms and Chaos,* International School of Physics Enrico Fermi, vol. 162, G. Casati, D. L. Shepelyansky, P. Zoller, G. Benenti, Eds. (IOS Press, Amsterdam, 2006), pp. 307–347.
13. C. W. J. Beenakker, H. van Houten, *Solid State Phys.* **44**, 1 (1991).
14. Y. Ji *et al.*, *Nature* **422**, 415 (2003).
15. Single-electrons detectors have been made but are yet too slow as compared with the electron transit time in the measurement leads.
16. B. J. van Wees *et al.*, *Phys. Rev. Lett.* **60**, 848 (1988).
17. D. A. Wharam *et al.*, *J. Phys. C* **21**, L209 (1988).
18. L. J. Geerligs *et al.*, *Phys. Rev. Lett.* **64**, 2691 (1990).
19. H. Pothier, P. Lafarge, C. Urbina, M. H. Devoret, *Europhys. Lett.* **17**, 249 (1992).
20. L. P. Kouwenhoven, A. T. Johnson, N. C. van der Vaart, C. J. P. M. Harmans, *Phys. Rev. Lett.* **67**, 1626 (1991).
21. A. Fujiwara, N. M. Zimmerman, Y. Ono, Y. Takahashi, *Appl. Phys. Lett.* **84**, 1323 (2004).
22. L. S. Levitov, H. Lee, G. B. Lesovik, *J. Math. Phys.* **37**, 4845 (1996).
23. T. Jonckheere, M. Creux, T. Martin, *Phys. Rev. B* **72**, 205321 (2005).
24. J. Keeling, I. Klich, L. S. Levitov, *Phys. Rev. Lett.* **97**, 116403 (2006).
25. J. Gabelli *et al.*, *Science* **313**, 499 (2006).
26. For additional experimental results, see G. Fève, thesis, Université Pierre et Marie Curie, Paris (2006), available at http://tel.archives-ouvertes.fr/tel-00119589.
27. M. Büttiker, H. Thomas, A. Prêtre, *Phys. Lett.* **A180**, 364 (1993).
28. M. Büttiker, A. Prêtre, H. Thomas, *Phys. Rev. Lett.* **70**, 4114 (1993).
29. A. Prêtre, H. Thomas, M. Büttiker, *Phys. Rev. B* **54**, 8130 (1996).

30. The Laboratoire Pierre Aigrain is the CNRS-ENS mixed research unit (UMR8551) associated with universities Paris 6 and Paris 7. The research has been supported by SESAME Ile-de-France and ANR-05-NANO-028 contracts.

Supporting Online Material

www.sciencemag.org/cgi/content/full/316/5828/1169/DC1
SOM Text
Figs. S1 and S2
References

13 February 2007; accepted 17 April 2007
10.1126/science.1141243

The Catalytic Cross-Coupling of Unactivated Arenes

David R. Stuart and Keith Fagnou*

The industrially important coupling of aromatic compounds has generally required differential prefunctionalization of the arene coupling partners with a halide and an electropositive group. Here we report that palladium, in conjunction with a copper oxidant, can catalyze the cross-coupling of *N*-acetylindoles and benzenes in high yield and high regioselectivity across a range of indoles without recourse to activating groups. These reactions are completely selective for arene cross-coupling, with no products arising from indole or benzene homo-coupling detected by spectroscopic analysis. This efficient reactivity should be useful in the design of other oxidative arene cross-couplings as well.

The immense scientific and commercial value of biaryl molecules is illustrated by their ubiquity as building blocks in light-emitting diodes, electron transport devices, liquid crystals, and medicinal compounds (*1*). The structural simplicity of biaryl compounds belies their preparative complexity, and the search for efficient and convergent syntheses has captivated the attention of synthetic chemists for more than a century. Over the past 30 years, biaryl cross-coupling reactions based on carbon fragment preactivation have revolutionized our ability to forge the carbon-carbon biaryl linkage (*1*, *2*). Of these reactions, the most widely accepted and used are the palladium-catalyzed cross-coupling reactions (such as the Suzuki reaction) of aryl halides and aryl organometallics (*3*). As is common today, these reactions are dependent on preactivation of the two aromatic carbon fragments with halides and electropositive groups, such as boronic acids or stannanes (*4*). Incorporation of these functional groups can require several synthetic steps,

Center for Catalysis Research and Innovation, University of Ottawa, Department of Chemistry, 10 Marie Curie, Ottawa, Ontario, Canada K1N 6N5.

*To whom correspondence should be addressed. E-mail: keith.fagnou@uottawa.ca